Diameter-Dependent Competitive Adsorption of Sodium Dodecyl Sulfate and Single-Stranded DNA on Carbon Nanotubes

Kunhua Lei,[†] Sergei M. Bachilo,[†] and R. Bruce Weisman[*, †, ‡]

[†] Department of Chemistry and the Smalley-Curl Institute, Rice University, Houston, Texas 77005, United States

[‡] Department of Materials Science and NanoEngineering, Rice University, Houston, Texas 77005, United States

ABSTRACT

The equilibrium compositions of coatings on single-wall carbon nanotubes were spectroscopically deduced for samples dispersed in dilute sodium dodecyl sulfate (SDS) and then exposed to low concentrations of ssDNA oligomers. With all studied oligomers, displacement of the SDS tended to occur at lower ssDNA concentrations for smaller diameter nanotubes than for larger diameter ones. However, the behavior varied significantly with oligomer. For example, the diameter dependence was steeper for $(TAT)_4$ than for $(ATT)_4$, suggesting that inter-strand head-to-tail hydrogen bonding interactions play a role in SWCNT wrapping. Concentrations of ssDNA in the range of several μg/mL displace SDS from nanotubes dispersed in 1500 μg/mL SDS solutions. This effect allows the use of coating exchange to prepare ssDNA dispersions with minimal oligomer costs. Another demonstrated use exploits the structure-dependent relative coating affinities in a simple filtration method for diameter enrichment of SWCNT mixtures.

TOC GRAPHIC

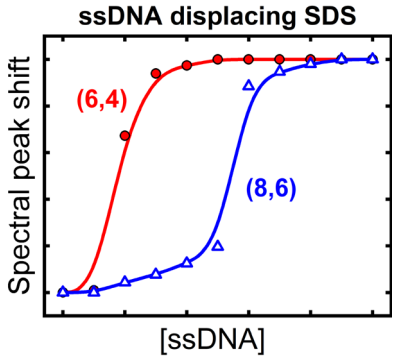

KEYWORDS nanotube coating displacement, spectroscopic titration, adsorption affinities, coating exchange, surfactant equilibria, diameter sorting, SDS

The unusual properties of single-wall carbon nanotubes (SWCNTs) have inspired extensive studies by many basic and applied researchers.[1–3] In most of that work, nanotube surfaces are noncovalently coated by one or more surfactants or polymers to allow individualization and the preparation of stable liquid suspensions.[4,5] These adsorbed coatings are also important because their specific interactions with SWCNTs are central to all major methods for structural sorting,[6–8] and they enable analyte selectivity in chemical sensing applications.[9,10] These key roles have motivated several investigations of coating displacement kinetics,[11–19] but equilibrium studies of relative coating stabilities or coating exchange remain much more limited.

Recently, Sims and Fagan have measured changes in SWCNT fluorescence intensities to study the equilibrated structure-specific exchange of alkyl and bile salt surfactants in the presence of polymers used in aqueous two-phase extraction sorting.[20] The rapid equilibration of those surfactants on nanotube surfaces allowed the use of a real-time spectroscopic titration method. Here we report a study of the SWCNT adsorption equilibrium for sodium dodecyl sulfate (SDS) in competition with short oligomers of single-stranded DNA (ssDNA). Such oligomers can show structure-specific interactions with SWCNTs and are valuable for nanotube sorting,[21,22] bio-sensing applications,[9,23] and band gap tailoring through the guanine functionalization reaction.[24,25] Because conformational relaxation of ssDNA on nanotubes can be quite slow, we performed "sampling" titrations in which a range of titrant (ssDNA) concentrations were added to multiple aliquots of an SDS dispersion. The samples were then incubated for several days to reach coating equilibrium, after which each was spectroscopically analyzed to give one point on a titration curve. The fluorescence data gave specific information on multiple SWCNT species, revealing that the adsorption competition between ssDNA and SDS depends on nanotube structure.

The basis of our approach is the sensitivity of SWCNT fluorescence to surface coating, which allowed us to monitor the displacement of one coating by another through emission spectroscopy. As described in detail in Experimental Methods, ten aliquots of an unsorted SWCNT suspension in 0.15% SDS were incubated for approximately ten days at room temperature after the addition of different amounts of ssDNA. We then measured SWCNT excitation-emission spectra for each of the equilibrated samples (e.g. Figure S2) and extracted sets of peak wavelengths and intensities for ten to twelve different semiconducting (*n*,*m*) species, using established spectral assignments.[26,27] To illustrate, Figure 1 shows emission slices, excited at 648 nm, for the original SDS dispersion and six of the equilibrated aliquots containing 0.5 to 3 μg of the $(ATT)_4$ ssDNA oligo. Systematic changes in peak intensities and peak wavelengths are evident.

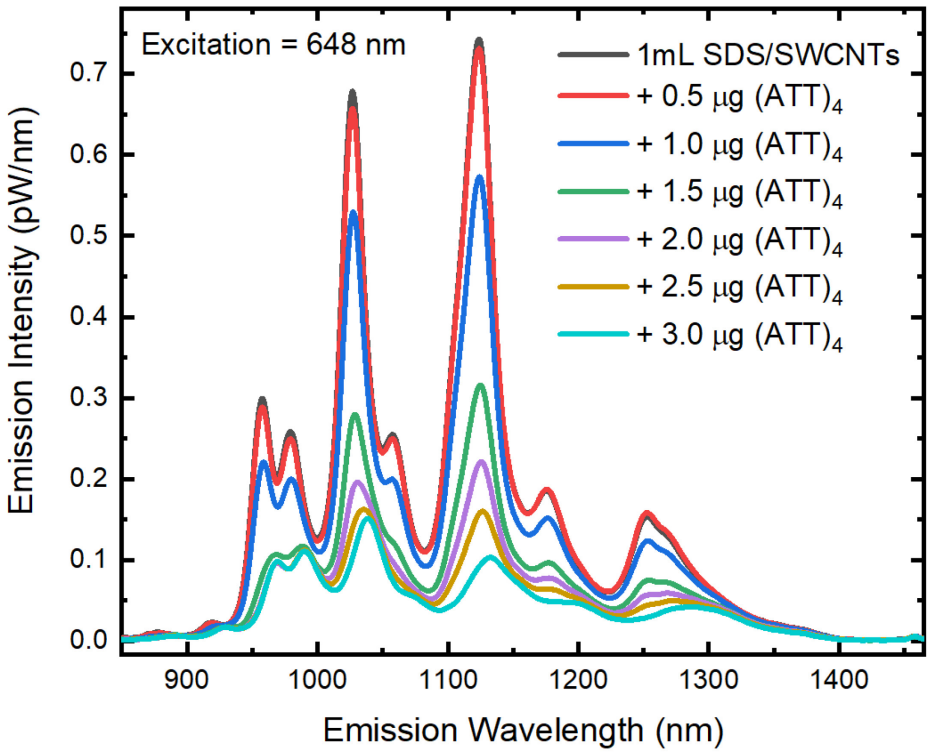

Figure 1. Emission spectra of equilibrated SWCNT dispersions in 0.15% SDS before and after addition of different masses of $(ATT)_4$ ssDNA, as shown in the legend. The fluorescence excitation wavelength was 648 nm and the sample volumes were 1.005 mL.

Figure 2a plots the emission peak wavelength shifts caused by $(TAT)_4$ addition for ten SWCNT species as a percentage of the maximum possible shifts, which are the measured differences between peak positions of dispersions prepared using pure $(TAT)_4$ as compared to 0.15% SDS solutions. All species show sigmoidal curve shapes, reaching asymptotic spectral shifts that range from 75 to 100% over the range of added ssDNA concentrations. In Figure 2b we plot

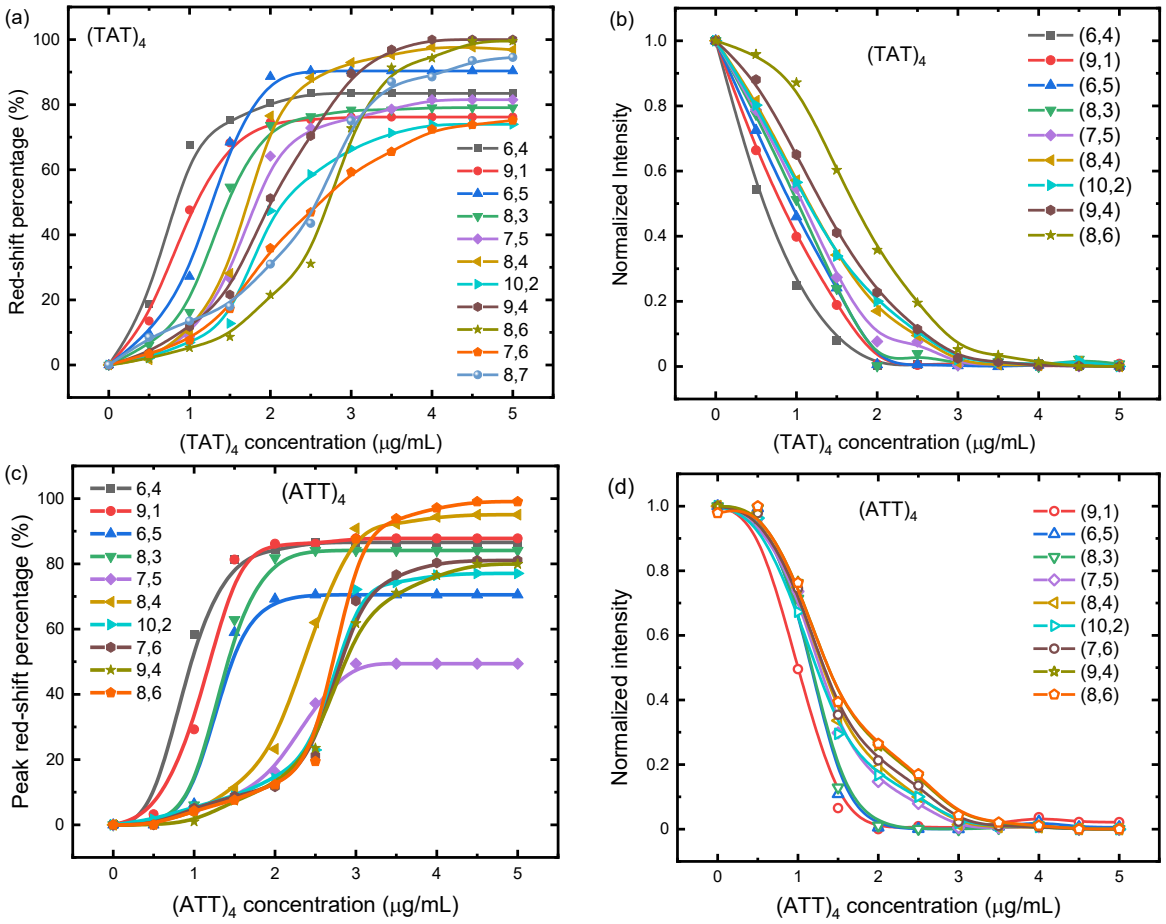

Figure 2. (a) Equilibrated spectral peak shifts for various (*n*,*m*) species as a fraction of the shift between peak wavelengths in pure SDS and pure $(TAT)_4$. The x-axis shows the added concentration of $(TAT)_4$. (b) Equilibrated peak intensities, normalized to the difference between values in pure SDS and pure $(TAT)_4$, plotted against added concentration of $(TAT)_4$. (c) Equilibrated spectral peak shifts for various (*n*,*m*) species as a fraction of the shift between peak wavelengths in pure SDS and pure $(ATT)_4$. The x-axis shows the added concentration of $(ATT)_4$. (d) Equilibrated peak intensities, normalized to the difference between values in pure SDS and pure $(ATT)_4$, plotted against added concentration of $(ATT)_4$.

the corresponding normalized intensities, calculated as $I_{norm} = \frac{I - I_{final}}{I_{initial} - I_{final}}$. These show much less sigmoidal character than the curves in Figure 2a. We attribute this shape difference to the nonlinear relation between SWCNT coverage and spectral shift arising from the much higher fluorescence quantum yields of SWCNTs coated by SDS as compared to ssDNA. The mismatch in quantum yields causes the overall emission spectrum of a sample equally coated by SDS and ssDNA to show a spectral peak located closer to the SDS position. This reduces the initial slopes of spectral shift curves (Figure 2a), distorting their shapes into a sigmoidal form. To more accurately infer coating displacements as a function of added ssDNA, we therefore use intensity data such as shown in Figure 2b. Spectral shifts and intensity changes induced by $(ATT)_4$ addition are plotted in Figures 2c and 2d.

It is apparent that the coating displacement titration curves in Figure 2 vary with SWCNT species. To efficiently characterize each of these spectral and intensity curves, we found the ssDNA concentration ($c_{1/2}$) that gave a response half-way between initial and final values. Figure 3a shows that there is a good correlation between these $c_{1/2}$ values for the $(TAT)_4$ intensity and spectral shift data, although the $c_{1/2}$ values are larger for spectra than for intensity because of the distortion effect described above. We note that the $(TAT)_4$ displacement trace for (6,5) does not appear unusual compared to other (*n*,*m*) species even though this oligo is a recognition sequence for (6,5).[28] Our titration results for $(GT)_6$, $(GT)_{12}$, $(GT)_{20}$, $(TTA)_4TT$, and $(GTT)_3G$ are shown in Figures S6 – S10.

In Figure 3c we plot the dependence of the $c_{1/2}$ intensity parameters on SWCNT diameter for four ssDNA oligos. The results for $(TAT)_4$, $(ATT)_4$, and $(GT)_6$, all of which have 12

nucleotides, show increases of $c_{1/2}$ with diameter. This implies that the thermodynamic stability of SDS coatings relative to the ssDNA coatings is lower for smaller diameter than for larger diameter nanotubes. $(GT)_{20}$, the longest oligo in the set, shows the same qualitative dependence on SWCNT diameter, but at mass concentrations that are greater by a factor of about 2. This difference may reflect an entropic free energy cost in $(GT)_{20}$ wrapping. We note that because of

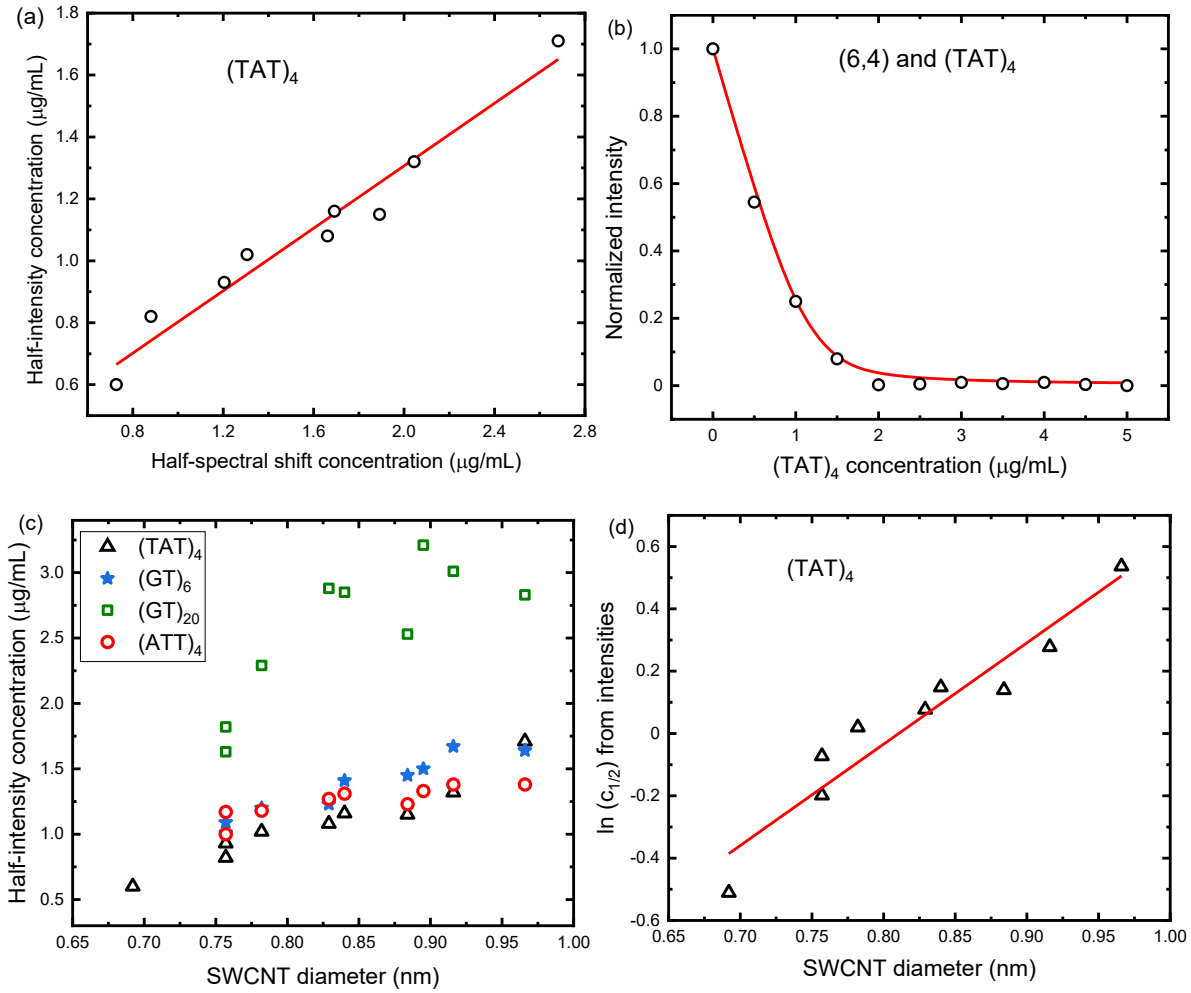

Figure 3. (a) Correlation plot showing the $(TAT)_4$ concentrations for each (n,m) that give half spectral shift and half intensity change. The line is a linear best fit. (b) Normalized peak intensity from (6,4) SWCNTs vs.oncentration of added $(TAT)_4$. Open circles show data points; the solid curve is a 2-parameter fit using a simple equilibrium model (see Supporting Information). (c) Values of concentrations giving half-intensity changes vs. SWCNT diameter for the four ssDNA oligos shown in the legend. (d) Natural log of the $(TAT)_4$ concentrations giving half-intensity changes plotted against nanotube diameter. The solid line is a linear best fit to the data points.

the low SDS concentration (0.15%) in our sample suspensions, the morphology of the displaced SDS coating is likely a monolayer with the dodecyl chains mainly aligned parallel to the nanotube axis.[29]

In Figure 2, the spectral shift and intensity data differ significantly for addition of $(ATT)_4$ compared to $(TAT)_4$. There is a milder diameter dependence for $(ATT)_4$ that can also be seen in Figure 3c. Note that the $(ATT)_4$ and $(TAT)_4$ oligos are isomeric; their only difference is that the end nucleotides of $(ATT)_4$ can base-pair with each other whereas those of $(TAT)_4$ cannot. We infer that inter-strand end pairing interactions reduce the variation of adsorption affinity with SWCNT diameter. Another difference between $(ATT)_4$ and $(TAT)_4$ displacement behavior is evident for (7,5). The asymptotic spectral shift for this species is 82% with $(TAT)_4$ but only 50% with $(ATT)_4$. To interpret this, we note that $(ATT)_4$ has previously been identified as a recognition sequence for (7,5),[28] and that a kinetic study found that sodium deoxycholate displaces $(ATT)_4$ from the two enantiomers of (7,5) at very different rates.[13] It therefore seems possible that the (7,5) trace in Figure 2c represents displacement of SDS only from the enantiomer with high $(ATT)_4$ affinity, with displacement from the low affinity enantiomer occurring either on a longer time scale or at higher concentrations than were used here. For both $(ATT)_4$ and $(TAT)_4$, many other (n,m) species show asymptotic spectral shifts between 70% and 90%. We suggest that for these nanotubes, surface regions remaining exposed after ssDNA wrapping are covered by SDS molecules, leading to blue-shifted emission as compared to nanotubes coated only by ssDNA.

Ideally, titration data would allow determination of equilibrium parameters for the SDS to ssDNA coating displacement reaction, represented in simplified form by eq 1.

$$(\mathrm{SDS}_n)/\mathrm{SWCNT} + \mathrm{DNA} \rightleftharpoons \mathrm{DNA}/\mathrm{SWCNT} + n\,\mathrm{SDS} \quad (1)$$

Here, DNA/SWCNT represents a nanotube segment coated with one strand of a ssDNA oligo; (SDS_n)/SWCNT represents the same segment coated with n molecules of SDS; DNA is a free ssDNA strand; and nSDS represents n free SDS molecules. Our system evidently contains thermodynamically distinct equilibria for all combinations of ssDNA oligo and SWCNT (n,m) species in the sample, with smaller diameter nanotubes having larger equilibrium constants. The complexity of multiple coupled equilibria unfortunately prevents us from extracting most quantitative parameters from the data. However, in the case of a small diameter SWCNT whose displacement occurs preferentially, we can check the relevance of eq 1 by using it to model the equilibrium coating displacement as a function of added ssDNA (see Supporting Information) and comparing the results to the measured intensity titration curve. The red curve in Figure 3b shows that this two-parameter simulation gives an excellent match to the measured (6,4) intensity changes caused by addition of $(TAT)_4$. Because our data were limited to one SDS concentration, it was not possible to separately determine the strongly coupled parameters n and the displacement equilibrium constant. Note that that many of the other measured intensity curves deviate qualitatively from the form of the simple simulations. We attribute this to the multiple simultaneous equilibria in which different SWCNT species compete for the same pool of ssDNA.

Despite these complexities, it is clear from our data that displacement of SDS is more thermodynamically favored for smaller as compared to larger diameter SWCNTs. Using the $c_{1/2}$ intensity parameters to characterize this pattern for $(TAT)_4$, we plot ln ($c_{1/2}$) against nanotube diameter in Figure 3d and find a nearly linear relation. As discussed in Supporting Information,

the slope of this curve indicates that the free energy change for SDS to $(TAT)_4$ coating exchange increases by approximately RT for a 0.3 nm increase in nanotube diameter. This thermodynamic diameter dependence of SDS-to-ssDNA coating displacement parallels the kinetic diameter dependence found recently for similar coating displacements.[19] There, the smaller diameter SWCNTs showed more rapid SDS displacements by ssDNA oligos, in cases where the oligos were short enough that conformational relaxation was not the rate limiting kinetic step.

Our data clearly show that ssDNA mass concentrations of several μg/mL can displace SDS from SWCNT surfaces at an SDS concentration of 1500 μg/mL. The amounts of ssDNA needed for half-displacement seem consistent with the prior experimental determination of an average ssDNA to SWCNT mass ratio of 1.0 in a SWCNT sample from the same HiPco batch used here.[30] The present findings suggest that it is feasible to prepare ssDNA-coated SWCNTs by first dispersing the nanotubes in dilute aqueous SDS, then adding small amounts of the much more expensive ssDNA, allowing time for the displacement equilibration, and finally filtering or dialyzing to remove SDS from the sample.

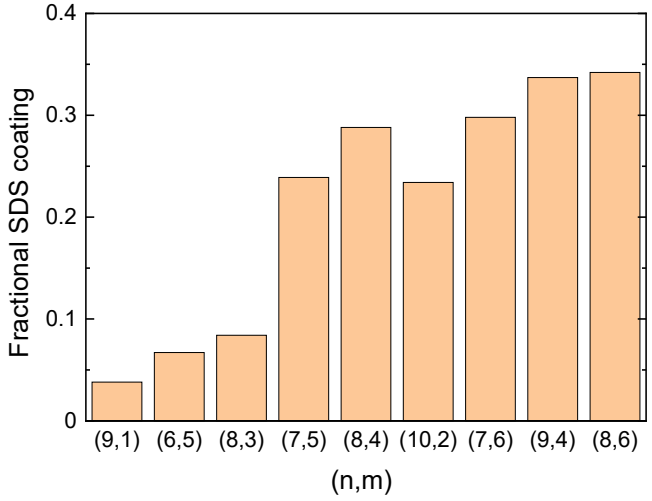

Figure 4. Estimated equilibrium SDS coverage for various (*n*,*m*) species after addition of 1.75 μg/mL of $(ATT)_4$ ssDNA.

Our data also suggest a rather simple approach to coarse structural sorting of SWCNTs, as low concentrations of $(ATT)_4$ can displace SDS more completely from the smaller diameter SWCNTs in a sample than from the larger diameter species. Figure 4 shows the fractional SDS coatings remaining at equilibrium, as estimated by interpolating the data for various (*n*,*m*) species in Figure 2c to find shift percentages at an $(ATT)_4$ concentration of 1.75 µg/mL. We demonstrated this scheme for generating diameter-dependent surface coatings by adding 1.75 µg/mL of the ssDNA oligo, allowing time for coating equilibration, and using quick centrifugal filtration to

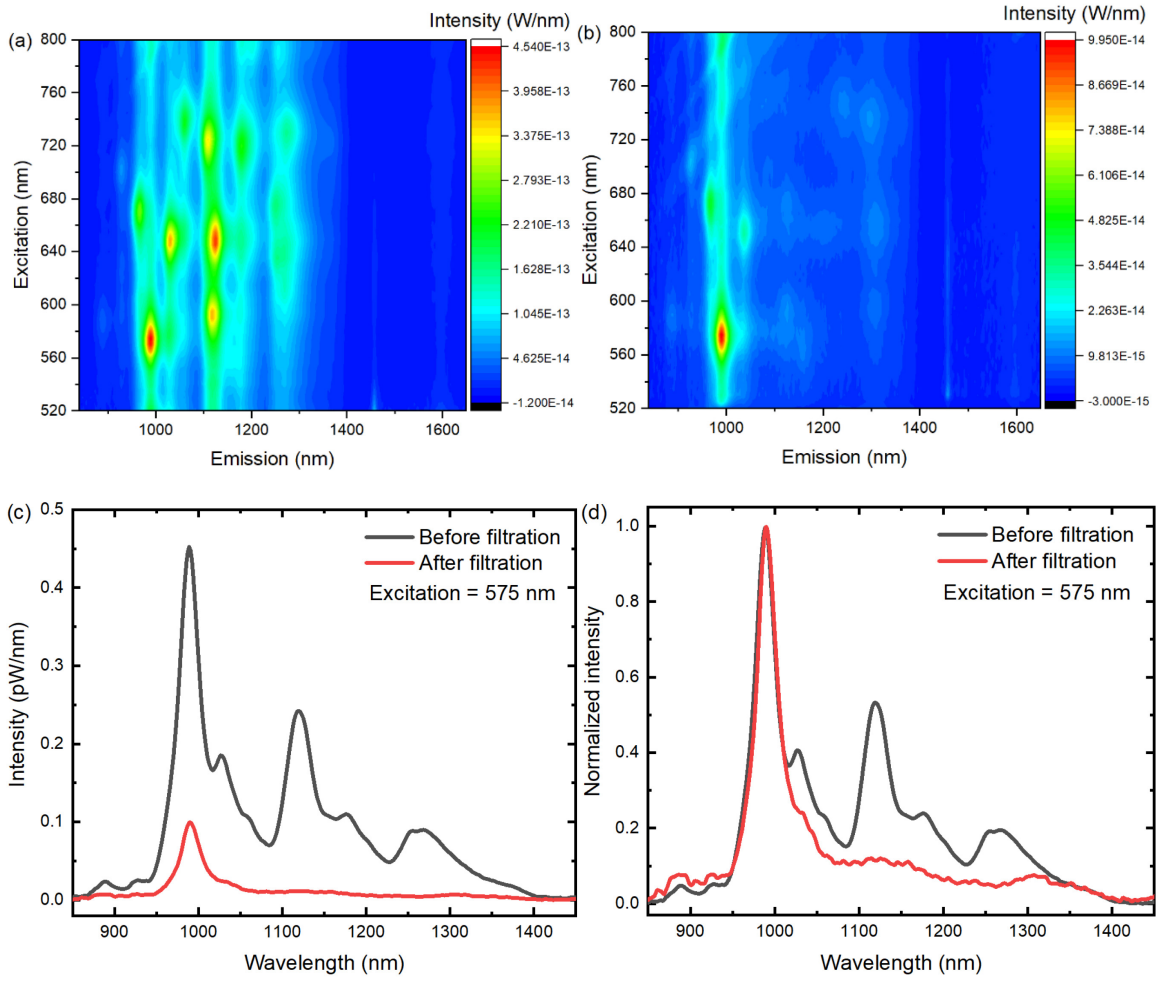

Figure 5. Excitation-emission maps of a SWCNT sample before (a) and after (b) processing for enrichment in small diameters. Note the different intensity color scales. The sample's emission spectra with 575 nm excitation are shown unnormalized in (c) and normalized in (d).

partially remove SDS solution from the sample before diluting it with water. The ssDNA-coated SWCNTs remained preferentially suspended and the recovered supernatant was enriched in the smaller diameter SWCNTs that were coated by $(ATT)_4$. Figure 5 shows spectra of a sample before and after this separation processing. It is clear that there was substantial enrichment in the smaller diameter SWCNTs relative to larger species. Consistent with the presumed mechanism, the peak positions of (6,4), (9,1), (6,5), and (8,3) were red-shifted compared to the SDS-coated starting dispersion, while peaks of larger diameter species remained nearly unshifted. We note that this initial implementation of displacement-based sorting gave low efficiency, with an estimated recovery yield of 7.4% for (6,5). Nevertheless, protocol refinements may lead to increased yields, and the simplicity and low cost of the approach may prove attractive for some applications.

In summary, we have used fluorescence spectroscopy to explore the competitive equilibrium adsorption of SDS versus short ssDNA oligomers on semiconducting single-wall carbon nanotubes. The results for oligomers $(ATT)_4$, $(TAT)_4$, $(GTT)_3T$, $(TTA)_4TT$, $(GT)_6$, $(GT)_{12}$, and $(GT)_{20}$ all show some dependence on nanotube diameter, with preferential displacement of SDS from smaller diameter SWCNTs as compared to larger diameter SWCNTs. No significant variation with nanotube chiral angle or mod(n-m, 3) identity was evident. Differences between the isomeric oligomers $(ATT)_4$ and $(TAT)_4$ point to a role for inter-strand head-to-tail hydrogen bonding interactions in stabilizing ssDNA coatings. In some cases, we also observe incomplete fluorescence peak shifts that suggest the presence of residual SDS at the nanotube surface, possibly in regions left exposed by the oligo wrapping. In the future, studies of this type can be extended by using sorted SWCNT samples to avoid competing equilibria among multiple species and allow the determination of free ssDNA concentrations and equilibrium parameters. Our findings show that ssDNA concentrations of several μg/mL can displace SDS coatings in samples dispersed in

0.15% (1500 μg/mL) SDS solutions. This may allow the preparation of ssDNA-coated samples with minimal cost for materials. Finally, we have demonstrated that the structure-dependent differences in coating affinities found here can be used in a very simple filtration method for diameter enrichment of SWCNT suspensions.

Experimental Methods

SWCNTs used in this study were taken from batch 195.1 produced by the Rice University HiPco reactor. To prepare pristine SDS-coated samples, we added weighed raw HiPco SWCNTs to a 0.15% (w/v) aqueous solution of sodium dodecyl sulfate (Acros). The SDS to SWCNT mass ratio at the beginning of sample preparation was kept at approximately 6:1 for all samples. The mixture was immersed in an ice water bath and tip-sonicated at 0.5 W/mL output power (3 mm tip, Misonix Microson XL) for 45 active min (90 min total with a duty cycle of 30 s on, 30 s off). The SWCNT suspensions were then centrifuged for 1.5 h at 13000×*g*. The top 80 percent of supernatant was collected, diluted with 0.15% SDS solution, and stored in sealed vials to give the SDS-coated SWCNT suspension used in a titration run. Based on near-IR absorption spectra and previously determined (*n*,*m*)-specific E_{11} absorption cross sections,[31,32] we estimate that many of the (*n*,*m*) species in the samples have concentrations in the range of 0.1 to 0.3 μg/mL.

We purchased custom-synthesized ssDNA oligonucleotides from Sigma-Aldrich, Inc. To prepare ssDNA solutions, 0.1 M NaCl solution was added to the tube containing known masses of ssDNA, and the tube was shaken to give complete dissolution. The ratio of DNA mass to NaCl solution was controlled to give a stock concentration of 1 μg/μL. The DNA stock solutions were kept refrigerated until use.

The absorption and near-infrared (NIR) fluorescence spectra of pristine SDS-suspended HiPco samples were measured in a 10×10 mm cell using a prototype model NS3 NanoSpectralyzer (Applied NanoFluorescence, LLC). Those fluorescence spectra were excited by diode lasers emitting at 532, 638, 671, and 779 nm. Full excitation-emission spectra of titrated samples were measured using a custom-built NIR spectrofluorometer. Its tunable excitation source was a spectrally filtered supercontinuum laser (SuperK Extreme, NKT Photonics), and NIR sample emission was detected by a TE cooled InGaAs array spectrometer (BWTek, Sol 1.7).

To perform a sampled titration, ten 1.00 mL aliquots of a SWCNT aqueous dispersion in 0.15% SDS were dispensed into ten cuvettes, each with dimensions of 10×10 mm. Different volumes of 1 μg/μL ssDNA oligo were added to the cuvettes (0.5, 1.0, 1.5, 2.0, 2.5, 3.0, 3.5, 4.0, 4.5, and 5.0 μL, except for $(GT)_{20}$, for which the added volumes were 1.7, 3.3, 5.0, 6.7, 8.3, 10.0, 11.7, 13.3, 15.0, 16.7, 18.3, and 20.0 μL). Additional volumes of aqueous 0.1M NaCl were used to keep the cuvette total volumes uniform (NaCl volumes were 4.5, 4.0, 3.5, 3.0, 2.5, 2.0, 1.5, 1.0, 0.5, and 0 μL, except for $(GT)_{20}$, for which they were 18.3, 16.7, 15.0, 13.3, 11.7, 10.0, 8.3, 6.7, 5.0, 3.3, 1.7, and 0 μL). After thorough mixing, the cuvettes were sealed with caps and then incubated for about ten days to allow equilibration, as indicated by stable spectra. After that we measured their SWCNT excitation-emission maps and used custom software to locate the peak excitation and emission wavelengths and intensities for multiple (*n*,*m*) species.

For the structural sorting, a 3 mL sample of SWCNTs suspended in 0.15% aqueous SDS was dispensed into an Eppendorf tube, followed by the addition of 3 μL of 2 μg/μL ssDNA solution. The tube was then securely capped, sealed with parafilm, thoroughly mixed, and incubated for 2.5 h in a water bath set at 36 °C. After that, the suspension was transferred into a centrifugal filter (Amicon, Ultracel YM-50, Cellulose 50,000 MWCO). The filter was then

centrifuged at 1000×*g* for 20 min. After centrifugation, the 100 μL of liquid suspension remaining above the membrane was collected and diluted to 1000 μL with 0.1 M NaCl solution. We characterized this diluted sample with an excitation-emission spectral scan.

ASSOCIATED CONTENT

Supporting Information. Description of the displacement equilibrium model; absorption and excitation-emission spectra of titrated samples; plots of (*n*,*m*)-specific excitation and emission peak wavelengths for titrated samples; spectral and intensity shift plots for titration with $(GTT)_3G$, $(GT)_{20}$, $(GT)_{12}$, $(GT)_6$, and $(TTA)_4TT$; illustration of filtration-based diameter sorting method.

AUTHOR INFORMATION

Corresponding Author

*E-mail: weisman@rice.edu. Tel: 713-348-3709

ORCID

Kunhua Lei: 0000-0003-1779-1315

Sergei M. Bachilo: 0000-0001-5236-1383

R. Bruce Weisman: 0000-0001-8546-9980

Notes

The authors declare the following competing financial interest: R.B.W. has a financial interest in Applied NanoFluorescence, LLC, which manufactures some of the instruments used in this project.

ACKNOWLEDGMENT

This research was supported by grant CHE-2203309 from the National Science Foundation.

References

(1) Iijima, S.; Ichihashi, T. Single-Shell Carbon Nanotubes of 1-nm Diameter. *Nature* **1993**, *363*, 603–605.

(2) Dresselhaus, M. S.; Dresselhaus, G.; Saito, R. Physics of Carbon Nanotubes. *Carbon* **1995**, *33*, 883–891.

(3) Saito, R.; Dresselhaus, G.; Dresselhaus, M. S. *Physical Properties of Carbon Nanotubes*; World Scientific Press: Singapore, 1998.

(4) O'Connell, M. J.; Bachilo, S. M.; Huffman, C. B.; Moore, V. C.; Strano, M. S.; Haroz, E. H.; Rialon, K. L.; Boul, P. J.; Noon, W. H.; Kittrell, C.; Ma, J. P.; Hauge, R. H.; Weisman, R. B.; Smalley, R. E. Band Gap Fluorescence from Individual Single-Walled Carbon Nanotubes. *Science* **2002**, *297*, 593–596.

(5) Moore, V. C.; Strano, M. S.; Haroz, E. H.; Hauge, R. H.; Smalley, R. E. Individually Suspended Single-Walled Carbon Nanotubes in Various Surfactants. *Nano Lett.* **2003**, *3*, 1379–1382.

(6) Arnold, M. S.; Green, A. A.; Hulvat, J. F.; Stupp, S. I.; Hersam, M. C. Sorting Carbon Nanotubes by Electronic Structure Using Density Differentiation. *Nat. Nanotechnol.* **2006**, *1*, 60–65.

(7) Liu, H. P.; Tanaka, T.; Kataura, H. One-Step Separation of High-Purity (6,5) Carbon Nanotubes by Multicolumn Gel Chromatography. *Phys. Status Solidi B-Basic Solid State Phys.* **2011**, *248*, 2524–2527.

(8) Fagan, J. A. Aqueous Two-Polymer Phase Extraction of Single-Wall Carbon Nanotubes Using Surfactants. *Nanoscale Adv.* **2019**, *1*, 3307–3324.

(9) Barone, P. W.; Baik, S.; Heller, D. A.; Strano, M. S. Near-Infrared Optical Sensors Based on Single-Walled Carbon Nanotubes. *Nat. Mater.* **2005**, *4*, 86–92.

(10) Zhang, T.; Mubeen, S.; Myung, N. V.; Deshusses, M. A. Recent Progress in Carbon Nanotube-Based Gas Sensors. *Nanotechnology* **2008**, *19,* 332001.

(11) Roxbury, D.; Tu, X.; Zheng, M.; Jagota, A. Recognition Ability of DNA for Carbon Nanotubes Correlates with Their Binding Affinity. *Langmuir* **2011**, *27*, 8282–8293.

(12) Shankar, A.; Mittal, J.; Jagota, A. Binding between DNA and Carbon Nanotubes Strongly Depends upon Sequence and Chirality. *Langmuir* **2014**, *30*, 3176–3183.

(13) Zheng, Y.; Bachilo, S. M.; Weisman, R. B. Enantiomers of Single-Wall Carbon Nanotubes Show Distinct Coating Displacement Kinetics. *J. Phys. Chem. Lett.* **2018**, *9*, 3793–3797.

(14) Jena, P. V.; Safaee, M. M.; Heller, D. A.; Roxbury, D. DNA-Carbon Nanotube Complexation Affinity and Photoluminescence Modulation Are Independent. *ACS Appl. Mater. Interfaces* **2017**, *9*, 21397–21405.

(15) Yang, Y.; Sharma, A.; Noetinger, G.; Zheng, M.; Jagota, A. Pathway-Dependent Structures of DNA-Wrapped Carbon Nanotubes: Direct Sonication vs Surfactant/DNA Exchange. *J. Phys. Chem. C* **2020**, *124*, 9045–9055.

(16) Xhyliu, F.; Ao, G. Chirality-Pure Carbon Nanotubes Show Distinct Complexation with Recognition DNA Sequences. *Carbon* **2020**, *167*, 601–608.

(17) Brunecker, F. K.; Schöppler, F.; Hertel, T. Interaction of Polymers with Single-Wall Carbon Nanotubes. *J. Phys. Chem. C* **2016**, *120*, 10094–10103.

(18) Alizadehmojarad, A. A.; Zhou, X.; Beyene, A. G.; Chacon, K. E.; Sung, Y.; Pinals, R. L.; Landry, M. P.; Vuković, L. Binding Affinity and Conformational Preferences Influence Kinetic Stability of Short Oligonucleotides on Carbon Nanotubes. *Adv. Mater. Interfaces* **2020**, *7*, 2000353.

(19) Lei, K.; Bachilo, S. M.; Weisman, R. B. Kinetics of Single-Wall Carbon Nanotube Coating Displacement by Single-Stranded DNA Depends on Nanotube Structure. *ACS Nano* **2023**, *17*, 17568–17575.

(20) Sims, C. M.; Fagan, J. A. Surfactant Chemistry and Polymer Choice Affect Single-Wall Carbon Nanotube Extraction Conditions in Aqueous Two-Polymer Phase Extraction. *Carbon* **2022**, *191*, 215–226.

(21) Zheng, M.; Jagota, A.; Strano, M. S.; Santos, A. P.; Barone, P.; Chou, S. G.; Diner, B. A.; Dresselhaus, M. S.; McLean, R. S.; Onoa, G. B.; Samsonidze, G. G.; Semke, E. D.; Usrey,

M.; Watts, D. J. Structure-Based Carbon Nanotube Sorting by Sequence-Dependent DNA Assembly. *Science* **2003**, *302*, 1545–1548.

(22) Ao, G.; Khripin, C. Y.; Zheng, M. DNA-Controlled Partition of Carbon Nanotubes in Polymer Aqueous Two-Phase Systems. *J. Am. Chem. Soc.* **2014**, *136*, 10383–10392.

(23) Heller, D. A.; Baik, S.; Eurell, T. E.; Strano, M. S. Single-Walled Carbon Nanotube Spectroscopy in Live Cells: Towards Long-Term Labels and Optical Sensors. *Adv. Mater.* **2005**, *17*, 2793–2799.

(24) Zheng, Y.; Bachilo, S. M.; Weisman, R. B. Controlled Patterning of Carbon Nanotube Energy Levels by Covalent DNA Functionalization. *ACS Nano* **2019**, *13*, 8222–8228.

(25) Zheng, Y.; Alizadehmojarad, A. A.; Bachilo, S. M.; Weisman, R. B. Guanine-Specific Chemical Reaction Reveals ssDNA Interactions on Carbon Nanotube Surfaces. *J. Phys. Chem. Lett.* **2022**, *13*, 2231–2236.

(26) Bachilo, S. M.; Strano, M. S.; Kittrell, C.; Hauge, R. H.; Smalley, R. E.; Weisman, R. B. Structure-Assigned Optical Spectra of Single-Walled Carbon Nanotubes. *Science* **2002**, *298*, 2361–2366.

(27) Weisman, R. B.; Bachilo, S. M. Dependence of Optical Transition Energies on Structure for Single-Walled Carbon Nanotubes in Aqueous Suspension: An Empirical Kataura Plot. *Nano Lett.* **2003**, *3*, 1235–1238.

(28) Tu, X.; Manohar, A.; Jagota, A.; Zheng, M. DNA Sequence Motifs for Structure-Specific Recognition and Separation of Carbon Nanotubes. *Nature* **2009**, *460*, 250–253.

(29) Tummala, N. R.; Striolo, A. SDS Surfactants on Carbon Nanotubes: Aggregate Morphology. *ACS Nano* **2009**, *3*, 595–602.

(30) Alizadehmojarad, A. A.; Bachilo, S. M.; Weisman, R. B. Compositional Analysis of ssDNA-Coated Single-Wall Carbon Nanotubes through UV Absorption Spectroscopy. *Nano Lett.* **2022**, *22*, 8203–8209.

(31) Streit, J. K.; Bachilo, S. M.; Ghosh, S.; Lin, C.-W.; Weisman, R. B. Directly Measured Optical Absorption Cross Sections for Structure-Selected Single-Walled Carbon Nanotubes. *Nano Lett.* **2014**, *14*, 1530–1536.

(32) Sanchez, S. R.; Bachilo, S. M.; Kadria-Vili, Y.; Lin, C.-W.; Weisman, R. B. (N,m)-Specific Absorption Cross Sections of Single-Walled Carbon Nanotubes Measured by Variance Spectroscopy. *Nano Lett.* **2016**, *16*, 6903–6909.